A Self-Folding Pneumatic Piston for Mechanically Robust Origami Robots

Chang Liu, Alec Orlofsky, Christa D. Kitcher, and Samuel M. Felton

***Abstract*—This letter presents a self-folding piston-style actuator for flat-foldable robots. Despite the variety of soft and planar actuators used in origami robots, extensional actuators are uncommon because they must resist buckling and bending loads, while soft and planar machines are inherently flexible. To address this, we developed a flat-foldable frame consisting of a piston and barrel that transforms into an operational state when driven by internal pressure. The barrel contains a pneumatic pouch and constrains the pouch to extend along a single axis for extensional actuation. We characterize the speed and blocked force of this actuator and compare it to a comparable unconstrained pouch in the actuation of a self-folding robotic arm. Our results indicate that the self-folding piston can operate much faster than the unconstrained pouch and resist off-axis loads.**

***Index Terms*—Mechanism design, hydraulic/pneumatic actuators, self-folding.**

I. Introduction

ORIGAMI engineering has been applied to a variety of challenges in robotics including mechanism design [1], [2], small-scale fabrication [3], fast and low-cost prototyping [4], [5], and transformable machines [6], [7]. Of particular interest to this letter are robots that can fold themselves from an inactive flat state to a functional 3D one [8], [9]. This capability has applications in logistics by enabling flat-pack robots, or autonomous construction in dangerous environments such as disaster zones or outer space [10], [11].

There are also many results indicating that origami engineering is well-suited for large-scale load-bearing applications. Folded sheets can create truss-like components, resulting in low-density, high-strength, and portable structures [12], [13]. However, these attractive mechanical properties have not been applied to self-folding robots. Existing robots are either too small (<50mm long) or too compliant to exert substantial forces or withstand substantial loads. For example, the largest untethered self-folding machine to date [14] was approximately 150mm long and could barely support its own weight while crawling. A larger, tethered self-folding robot arm [15] was actuated with pneumatic pouch motors, but the actuators were slow and susceptible to off-axis forces.

A critical limitation to large self-folding machines is their operational actuators – the actuators used after the folding process to locomote, manipulate, or otherwise function. Some origami robots use traditional actuators such as electric motors [14], but these discrete components cannot be folded flat. Other origami machines have used a wide variety of planar, flexible, and soft actuators to fit within a flat form, and we can categorize them as contractile, bending, or extensional. There are many promising contractile actuators including shape memory alloys [16], [17], pneumatic McKibben-style [18], [19] and origami-inspired [20] actuators, and motor-driven tendons [21], [22]. One high-force example is a vacuum-driven origami design that can exert up to 428 N [23]. There are also soft and planar bending actuators, including soft pneumatic actuators [24], [25] and piezoelectric bending actuators [26]. Some designs have combined these soft actuators with rigid frames in order to guide their kinematics and resist off-axis forces [27], [28], including the use of bio-inspired 'skeletons' [29].

However, there are few extensional actuators, and this is because when an actuator applies an extensional force, it experiences a reactive compressive force that can induce buckling. Soft and planar actuators are inherently vulnerable to bending and buckling because of their low rigidity, due either to low material stiffness or small second area moment [30]. For example, the self-folding arm mentioned above used an unconstrained pouch motor for actuation, but the cross-section of the pouch (177cm^2) had to be much larger than its contact surface (58cm^2) to prevent buckling [15], making it slow and inefficient. Other extensional actuators have reported similarly low bending stiffnesses [31].

Linearly-extending deployable structures produce extensional motion but there are certain design limitations in existing approaches that make them unsuitable for this application. Many designs use repeating folding elements [32]–[34], but these structures don't scale up well because the large number of joints (creases) decrease the stiffness of the overall structure. Other mechanisms use locking features to increase rigidity and are only stiff when fully folded [22].

In this letter we propose a foldable piston that integrates a soft pneumatic pouch motor [19], [35] with a foldable structural element to create a low-profile, high-force, and mechanically robust actuator that can be integrated with self-folding machines (Fig. 1). The piston architecture resists off-axis loads and constrains the pouch to expand along a single axis,

Manuscript received September 7, 2018; accepted January 12, 2019. Date of publication January 29, 2019; date of current version February 15, 2019. This letter was recommended for publication by Associate Editor D. Lau and Editor P. Rocco upon evaluation of the reviewers' comments. This work was supported by Northeastern University. *(Corresponding author: Samuel M. Felton.)*

The authors are with the College of Engineering, Department of Mechanical and Industrial Engineering, Northeastern University, Boston, MA 02115 USA (e-mail: liu.chang7@husky.neu.edu; orlofsky.a@husky.neu.edu; kitcher.c@husky.neu.edu; s.felton@northeastern.edu).

This letter has supplementary downloadable material available at http://ieeexplore.ieee.org, provided by the authors.

Digital Object Identifier 10.1109/LRA.2019.2895881

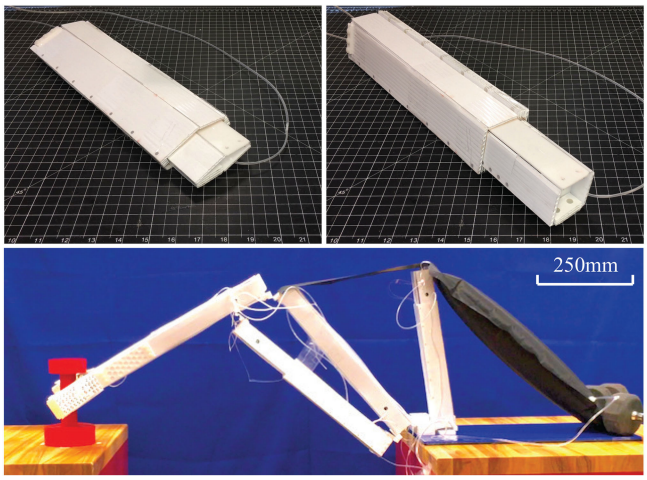

Fig. 1. This letter presents a self-folding piston that can apply extensional force and resist off-axis loading. We demonstrate its capabilities by integrating it into a self-folding robot arm. Grid lines are 1.25 cm apart.

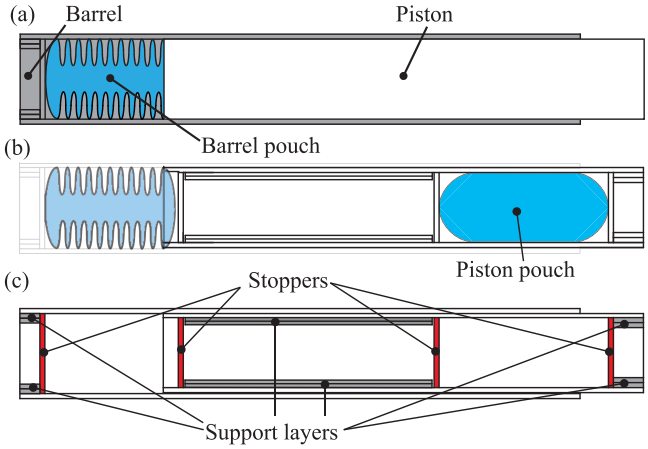

Fig. 2. (a) The self-folding actuator consists of three components: an outer barrel (gray), an inner piston (white), and a barrel pouch between the two (blue). (b) A second pouch (blue) is embedded within the piston. The two pouches inflate simultaneously to drive the folding process. (c) Stoppers (red) lock the fold pattern into place, while support layers (gray) are used to increase the actuator's rigidity and prevent the stoppers from rotating more than 90°.

improving speed and efficiency. We characterize the actuator's performance through physical experiments and compare it to a completely soft pneumatic actuator in the operation of a self-folding robot arm.

By designing and building this piston, we demonstrate three design principles for foldable extensional actuators. (1) A single prismatic joint in an origami structure can resist substantial buckling and bending loads. (2) Sliding prismatic joints require geometric precision, and this can be achieved through parallel fold patterns with a single degree of freedom (DOF). (3) Repeatable inflation of pneumatic pouches in constrained volumes is feasible with distributed buckling of the pouch walls to prevent folding and twisting.

II. Design and Fabrication

The actuator consists of three operational components: an outer barrel, an inner piston, and a pneumatic pouch within the barrel (Fig. 2a). The barrel and piston fold flat, with the piston and pouch fitting inside the barrel in the flat state. An additional pouch is embedded within the piston to drive self-folding (Fig. 2b). The fold pattern is inspired by previous examples of fluidic origami [23], [36], and the benefits of this approach are explored in a previous demonstration of a self-folding arm [15]. To summarize these benefits, the limited degrees of freedom and closed kinematic chains in the fold pattern improve precision, reliability, and structural integrity.

The barrel and piston consist of four rigid walls connected by flexural hinges. Stoppers are connected to the inner faces of the walls by flexural hinges. These stoppers fold to fit within the cross-section of the barrel or piston and hold the walls in a square shape. Additional support layers are attached to certain areas on the walls to increase stiffness and prevent the stoppers from overfolding (Fig. 2c). The walls, support material, and stoppers are made of 3.2mm thick corrugated polypropylene (CPP) and the flexural hinges are heavy duty shipping packaging tape (SPT).

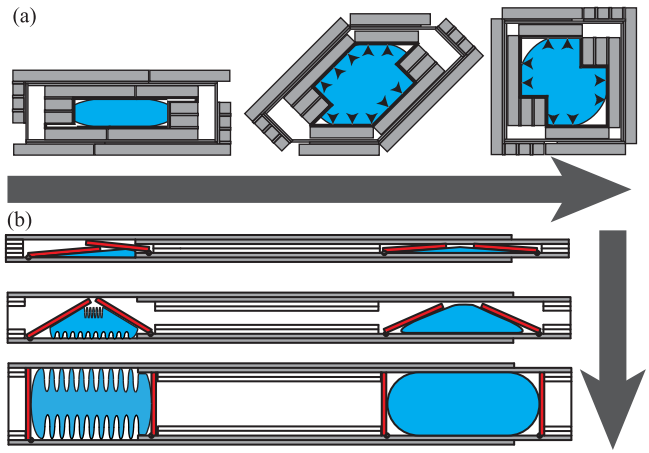

Fig. 3. (a) The actuator transforms through a pop-up style fold pattern in which the barrel and piston walls (gray) start parallel, and are pushed into a perpendicular position by embedded pneumatic pouches (blue). (b) Simultaneously, the pouches push up stoppers (red) that fit into the barrel and piston cross-sections, locking the walls into position.

The piston is four layers thick when folded flat (Fig. 3a). The two outer layers form the walls and the two inner layers contain the stoppers and support material. The inner layers also include gaps that leave room for the piston pouch when the piston is flat. The barrel has a similar design but includes two extra layers to create a larger cavity and make room for the piston (Fig. 3a). Overhanging portions on two of the walls prevent the barrel from folding beyond 90°. The barrel includes a thin fiberglass layer along the inner surface to reduce friction between the barrel and the piston. This layer replaces SPT as the flexural hinges between the walls.

During the folding process, the barrel and piston pouches are pressurized simultaneously, causing them to expand and exert a force on the walls of the barrel and piston (Fig. 3). This pushes the longitudinal walls of the assembly to fold into

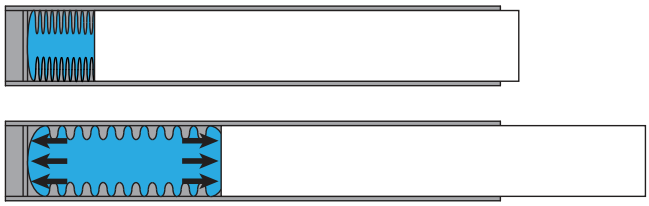

Fig. 4. When the barrel pouch is pressurized it applies force to the piston, extending it out of the barrel.

their operational position and pushes the stoppers up and into the barrel and piston cross-sections, locking them into their operational shape.

During operation, the barrel pouch is pressurized and pushes against the barrel and stopper, forcing them apart and actuating the assembly (Fig. 4). The barrel constrains the piston to a single DOF and forces the pouch expansion along a single axis, allowing for greater speed and efficiency than an unconstrained pneumatic pouch. The operational dimensions of the piston are 280mm long, 45mm tall and 45mm wide, and the dimensions of the barrel are 355mm long, 60mm tall and 60mm wide. When folded flat, the assembly has a thickness of 20mm and a mass of 92g.

A. Barrel and Piston Fabrication

The barrel and piston were fabricated separately using a similar process (Fig. 5a-b). The structural layers (beam walls, support layers, and stoppers) were machined using a CO_2 laser cutter. Support layers were bonded to the beam walls using double sided adhesive transfer tape (ATT) and stoppers were attached with SPT, forming flexural hinges between the stoppers and the walls. For the piston, the beam walls were joined using SPT to create hinges between the walls. The piston pouch was placed beneath the stoppers in the piston. The distal edges of the walls were then connected with SPT to produce a closed-loop structure. For the barrel, a single sheet of polytetrafluoroethylene-coated fiberglass adhesive tape acted as the flexural layer instead of SPT, and this sheet was bonded to the walls with ATT. In both elements, holes were cut through the outer and support layers at the two edges where the outer and support layers were connected. Hot glue was injected through these holes and spread between the layers, increasing the adhesive strength between the layers at these edges.

B. Pouch Fabrication

The pouches were fabricated by sealing two taffeta sheets (0.008" thick) into a rectangular shape with an impulse heat sealer. We chose taffeta over other materials (e.g., nylon) because it is heat-sealable and high-strength, and we used a rectangular shape because it is relatively straightforward to heat-seal. A small opening was left on the side of the pouch for inserting a tube fitting. The tube fittings were made using 0.125" long 10-32 nylon screws, nuts, and 0.063" 90° tube fitting. A hole was drilled in the center of each screw using a 2.3mm drill bit, and a 0.063" 90° tube fitting was plugged in and sealed using Loctite 416. The "home-made" tube fitting was screwed into the pouch and sealed using Loctite 416.

The barrel pouch includes elastic elements (Pale Crepe Gold Rubber Bands, Size 74, 0.75" wide $\times$ 3.5" long) bonded to the inner wall of the pouch with Loctite 4851. The elements were aligned along the long axis of the pouch and attached at regular increments along the wall by first folding the taffeta and then selectively bonding the elements to the inner surface (Fig. 6a). This ensured that the pouch collapses evenly in an accordion-like geometry, allowing it to expand and contract without folding over on itself (Fig. 6b). We observed that inelastic pouches would often crease in such a way that would either prevent it from fully inflating or cause sudden jumps in the piston position.

Once the pouch was fabricated, the components were assembled by inserting the pouch and the piston into the barrel in their folded state (Fig. 5c). The pouch was attached to both the piston and barrel, limiting the maximum stroke and providing a restoring force when the barrel pouch was deflated. The actuator was then folded flat. The fabrication process for a single piston took 100 minutes of labor and 12 hours for the glue to dry.

C. Arm Design

To demonstrate the functionality of this actuator, we integrated two pistons into a 2-DOF self-folding robotic arm (Fig. 7). The arm design is similar to a previous demonstration [15] that was actuated by unconstrained pouch motors. In the new design, the piston actuators are under longitudinal compression and must resist buckling, demonstrating their rigidity. In addition, the arm segments of the new design were elongated to 50cm (from a previous length of 38cm) to demonstrate greater reach.

Each arm segment consists of a self-folding beam with a similar design and fabrication process as the piston. The two segments are connected by a rotary joint consisting of 10 acrylic layers to accommodate the linear actuator that lies between them in the flat position. The bottom segment is connected by another rotary joint to ground, which in this case is an acrylic base plate. We refer to these two joints as the elbow and shoulder, respectively.

One actuator drives the elbow and the other is combined with a tendon assembly to drive the shoulder. When the arm is flat, the two beams and two actuators lie on top of each other. In this form it consists of 32 layers stacked vertically. A pouch is located underneath the folded structure that pushes the arm into an operational position as it inflates. This push-up pouch doubles as one of the tendons that drives the back beam in the arm. The actuators are driven by two pneumatic pumps (Karlsson Robotics, AIRPO D2028B, 1101-0183) for inflation and one pump for deflation. Seven miniature electric valves (ASCO 411L2112HVS - 2/2 NC) are used to control flow direction.

A gripper consisting of two L-shaped fingers is attached to the end of the arm. The gripper is made from acrylic, and each finger is attached to the arm by a single rotary joint. The gripper is actuated by a pouch motor between the fingers, which is driven by an additional pump and valve.

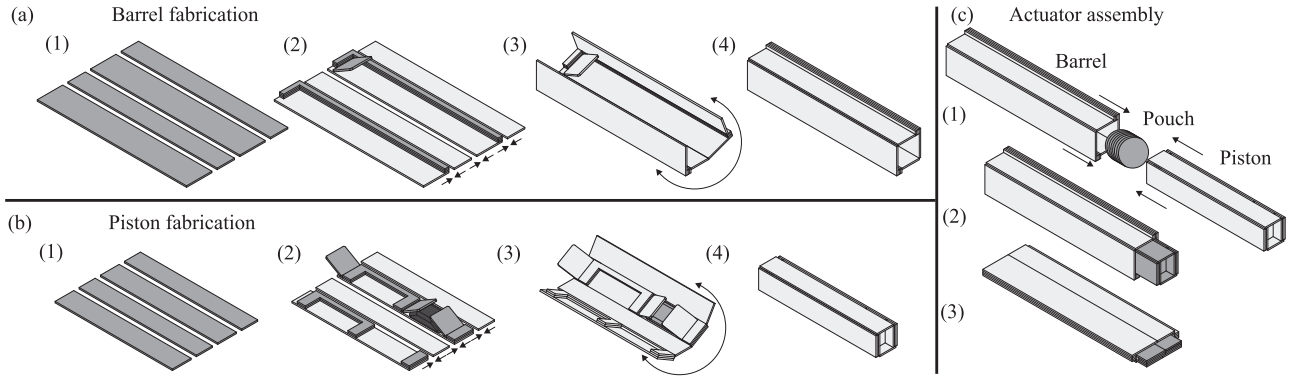

Fig. 5. Fabrication steps for the linear actuator. (a) The barrel is fabricated in four steps: (1) The four outer walls are laser-cut, (2) support layers and stoppers are cut and installed on the walls, (3) the walls are connected via tape, creating flexural hinges between the walls, and (4) The barrel is folded up and the two edges are joined with another tape hinge. (b) The piston is fabricated in a similar process, but a pouch is installed under the stoppers in step (2). (c) The pouch and piston are inserted into the barrel, and the entire assembly is folded flat.

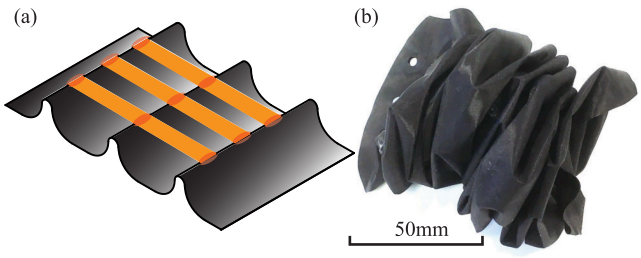

Fig. 6. (a) Elastic elements were prestreched and selectively bonded to the inner surface of the pouch at regular intervals. (b) This gave the pouch an accordian-like shape that was necessary for the pouch to expand and contract linearly with pressure.

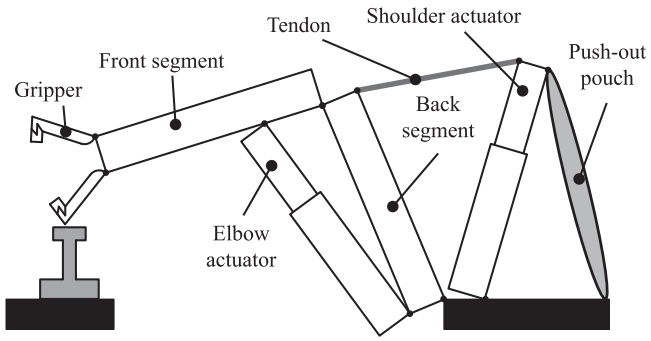

Fig. 7. The self-folding arm consists of two structural beams: the front beam is driven directly by a linear actuator and the back beam is driven by a linear actuator combined with a tendon assembly. The arm includes a gripper made up of two open-faced L-shaped structures.

The assembled arm weighs 0.9kg and the pumps and valves required to drive it weigh and additional 1.5kg.

III. Experiments and Results

A. Blocked Force Measurements

To characterize the actuator force, we measured it using a force sensor (TE Connectivity Measurement Specialties, MEAS FC2231-0000-0100-L) when the piston was blocked at three different positions: 80 mm, 140 mm, and 200 mm. Five samples were tested at each position and a pressure sensor (Balluff, BSP004J) measured the pressure in the pouch. We compared

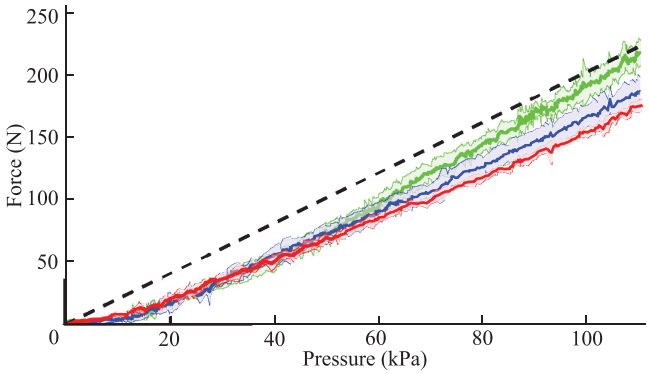

Fig. 8. The force of the linear actuator was measured as a function of pouch pressure (solid lines, shaded regions indicate standard deviation, N = 5) and plotted along with the predictive model (dashed lines). Black: extension of 200 mm, Blue: extension of 140 mm, Red: extension of 80 mm.

these results to a model that assumes the pressure is applied evenly across the cross-section of the operational pouch so that $F = P\pi r^2$, where F is the force exerting by the piston, P is the pressure in the pouch, and r is the cross-sectional radius of the pouch.

Results show a linear relationship between force and pressure that matches model predictions (Fig. 8). The resulting force was slightly less than what was predicted by the model, and we believe that this is caused by the friction between the pouch and inner surface of the barrel. Although the fiberglass minimizes the friction, deformation in the barrel walls will still result in some resistive forces. The experimental results also indicate the actuator performs better as the piston displacement increases. We believe that this is because the pouch becomes less twisted and better matches its ideal shape as it expands.

B. Free-Displacement Speed

To characterize the actuator speed, the piston displacement was measured as a step input was applied to the pressure with three different magnitudes: 70kPa, 140kPa, and 210kPa (Fig. 9). Three samples were tested for each magnitude. In all experiments, the displacement settled at approximately 250mm. The

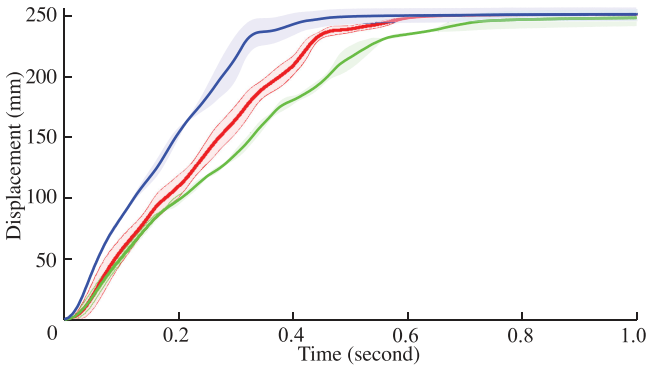

Fig. 9. Displacement of the piston as a function of time when a step input pressure is applied to the actuator. Three step pressures were used: 70 kPa (black), 140 kPa (red), and 210 kPa (blue). Shaded regions indicate standard deviation, N = 3.

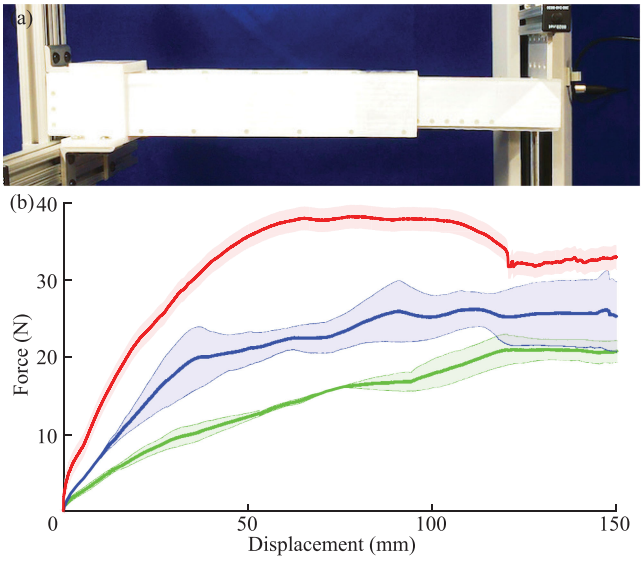

Fig. 10. (a) The cantilever loading experiment. (b) The displacement of the actuator tip was plotted as a function of load for three piston positions: 200 mm (black), 140 mm (blue), and 80 mm (red). Shaded regions indicate standard deviation, N = 3.

rise times (to 90% of steady-state) for each set of experiments were 0.62s, 0.43s, and 0.31s respectively.

C. Bending Stiffness Measurements

To characterize the actuator's stiffness against off-axis loads, we rigidly fixed the barrel and applied a point force F to the piston 20mm from its tip using a Mecmesin material tester (Multitest 2.5-i). We plotted the deflection δ of the tip as a function of F for three piston extensions x_e: 80mm, 140mm, and 200mm (Fig. 10). Three samples were tested for each displacement.

We observed a small region of linear elasticity, after which the barrel walls buckled at the rigidly fixed end. Under further displacement, this buckling lead to a drop in maximum load, as evidenced by the decrease in force seen in the 80mm position at 120mm displacement. We characterized the bending stiffness k_b of the beam at each extension by fitting the cantilever displacement equation $\delta = FL^3/3k_b$ to the linear region, where

TABLE I
PISTON STIFFNESS AS A FUNCTION OF EXTENSION

Extension x_e (mm)	80	140	200
Bending stiffness k_b (N·m^2)	29.37	24.45	19.05

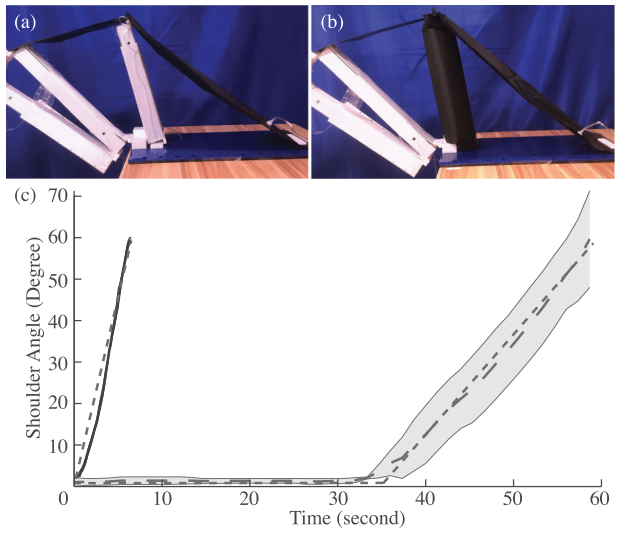

Fig. 11. (a) The shoulder joint actuated by the piston-style actuator. (b) The same joint actuated by the unconstrained pouch motor. (c) The angular displacement of the shoulder joint when actuated by the piston-style actuator (solid line) and the unconstrained pouch motor (dashed line). The slopes of the dotted lines represent the angular speed. Shaded regions indicate standard deviation, N = 3.

$L = 350\text{mm} + x_e$ is the total piston length (Table I). We found that k_b decreases as x_e increases, likely due to the decreasing overlap between the piston and the barrel.

D. Comparison With Pouch Motor

To compare the piston-style actuator with an unconstrained pneumatic pouch, we installed each actuator at the shoulder joint of our self-folding arm (Fig. 11) and measured the angular speed in response to a pressure step input of magnitude 70kPa. In order to prevent buckling, the pouch motor had to have a cross-sectional area of 81cm^2 and an internal volume at maximum displacement of 4942cm^3, compare to the barrel pouch cross-sectional area of 20cm^2 and volume of 514cm^3. Because of these differences, we expected that the piston-style actuator would be substantially faster. Three actuators of each type were tested in a single shoulder joint.

The piston-style actuator demonstrated a faster actuation speed of 9.75°/s, compared to a speed of 2.29°/s from the pouch motor (Fig. 11). In addition, the pouch motor took 35s to begin actuation because a substantial mass of air had to fill the pouch before it even began to apply force to the tendon assembly and drive the shoulder. This 'charging' period corresponds to the self-folding period of the piston assembly which normally occurs during self-folding, not operation. However, even if we compare these directly, the piston takes five seconds, a substantially shorter time due to the smaller internal volume. These results indicate that the piston-style actuator performs better in the robotic arm.

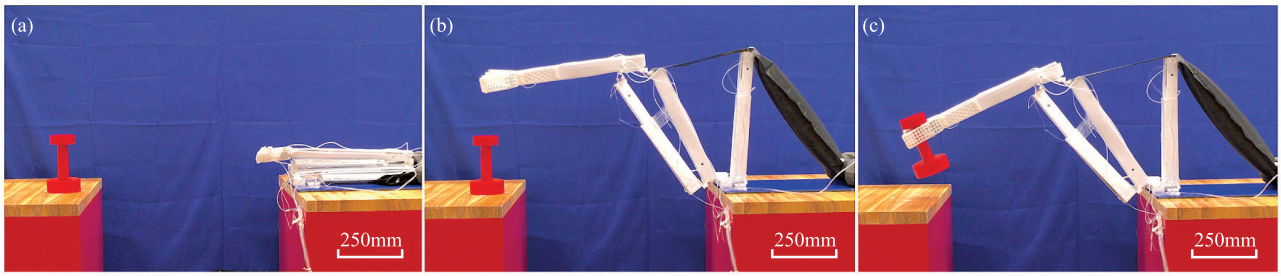

Fig. 12. The self-folding process and grasping motion of the arm. (a) The arm in its flat configuration. (b) The arm after folding into its operational state. (c) The arm lifting the dumbbell. The supplemental video shows the full operation.

TABLE II
COMPARISON OF TRADITIONAL AND SELF-FOLDING PISTON

Actuator	Thickness	Stroke	Mass	Force	Pressure
Speedaire 5PEH8 [37]	19 mm	250 mm	231 g	300 N	1030 kPa
Self-folding piston	19 mm (flat)	250 mm	92 g	200 N	105 kPa

E. Self-Folding Arm

The robotic arm self-folded and performed a grasping motion (see Supplemental Video). The arm was initially deflated and folded into a flat configuration 15cm tall. A 1.5kg dumbbell was placed 90cm away from the arm (Fig. 12a). First, the beams and pistons self-folded into their operational form. Next, the pistons moved the arm closer to the dumbbell while the gripper opened (Fig. 12b). The robot grasped and lifted the dumbbell (Fig. 12c), then put it back down. During self-folding and operation, the maximum pneumatic pressure was 200kPa.

IV. DISCUSSION

Compared to traditional pistons, the self-folding design has several advantages. For comparison, we selected the Speedaire 5PEH8 [37], a piston with the same stroke length and thickness as the self-folding piston in its flat state (so that its form factor would fit in the flat-folded arm). While the traditional piston has 50% greater force generation, it requires 10 times the operating pressure and weighs over twice as much, indicating that self-folding piston has a better stroke energy density (Table II).

Compared to deployable structures, experimental results indicate that the self-folding piston is substantially stiffer over its full range. As one example, Filipov et al. [34] built a linear-deployable origami beam with a mass of 10g and applied a three-point bending load. Using their results, we calculated that the beam bending stiffness k_b when fully extended was $1.63\text{N} \cdot \text{m}^2$ and the stiffness-to-weight ratio was 16.6, which is less than but comparable to the 21.1 ratio for the piston. However, at shorter lengths the deployable beam stiffness-to-weight ratio decreased substantially, down to 0.02 at 50% extension, while the piston stiffness goes up as the length goes down.

There are some practical limitations to the current design. The maximum pressure and actuator force are limited by the burst pressure of the pouch and tensile strength of the flexural hinges. The maximum size is limited by the buckling threshold of the walls. If the length and width of the actuator are increased, the buckling threshold decreases, making the actuator weaker against compression and bending loads. The minimum size is limited primarily by fabrication processes and material selection. Specifically, our heat-sealing process is imprecise and requires a border around the pouch. Although different materials and fabrication methods could be used, they would have to be sufficiently flexible or compressible to fold flat. Despite these challenges, we expect that this design will be easier to scale than other options (such as the deployable structures mentioned above) because of its favorable stiffness and simple design.

We expect that the barrel pouch can be redesigned to reduce its collapsed size. The accordion pattern cannot be flattened as well as a flat sheet, so an alternative design that can still freely expand and contract would be preferable. In addition, the stroke of the actuator is limited to a fraction of the barrel length, which cannot be reduced through folding. Traditional pistons use a multi-stage architecture to increase maximum displacement, but the tolerances would need to be much tighter than we have currently demonstrated.

Future work may investigate how this design can be integrated into other platforms and applications. Many robotic systems use linear actuators, including parallel delta robots [38], cartesian manipulators [39], and tensegrity robots [40]. Many of these applications require precise position control, so an encoder- or potentiometer-based sensor could be integrated along the barrel's inner surface for feedback control. Depending on the application, alternative actuation methods may also be studied. We chose positive pressure pneumatics because we were already using them to drive self-folding and they can output arbitrarily high forces, but similar designs could be driven by negative pressure or tendons.

V. CONCLUSION

This letter demonstrates that a prismatic joint can be built into a flat-foldable machine using parallel fold patterns, and it can be repeatably actuated with a pleated pouch design. The results indicate that an origami piston outperforms an unconstrained pneumatic pouch in two ways: (1) it can resist off-axis loads, and (2) it has a faster response time. Given that there are few options for extensional actuators in flat-foldable robots and the many uses of piston-based actuation in traditional machines, we believe that this design fills an important gap in origami robot design.

REFERENCES

[1] E. vander Hoff, D. Jeong, and K. Lee, "OrigamiBot-I: A thread-actuated origami robot for manipulation and locomotion," in *Proc. IEEE/RSJ Int. Conf. Intell. Robots Syst.*, 2014, pp. 1421–1426.

[2] Z. Zhakypov, M. Falahi, M. Shah, and J. Paik, "The design and control of the multi-modal locomotion origami robot, tribot," in *Proc. IEEE/RSJ Int. Conf. Intell. Robots Syst.*, 2015, pp. 4349–4355.

[3] X. Ma, D. Vogtmann, and S. Bergbreiter, "Dynamics and scaling of magnetically folding multi-material structures," in *Proc. IEEE Int. Conf. Robot. Autom.*, 2016, pp. 1899–1906.

[4] H. Shigemune, S. Maeda, Y. Hara, U. Koike, and S. Hashimoto, "Kirigami robot: Making paper robot using desktop cutting plotter and inkjet printer," in *Proc. IEEE/RSJ Int. Conf. Intell. Robots Syst.*, 2015, pp. 1091–1096.

[5] A. Mehta *et al.*, "A design environment for the rapid specification and fabrication of printable robots," in *Experimental Robotics*. Berlin, Germany: Springer, 2016, pp. 435–449.

[6] P. M. Kornatowski, S. Mintchev, and D. Floreano, "An origami-inspired cargo drone," in *Proc. IEEE/RSJ Int. Conf. Intell. Robots Syst.*, 2017, pp. 6855–6862.

[7] F. Zuliani, C. Liu, J. Paik, and S. M. Felton, "Minimally actuated transformation of origami machines," *IEEE Robot. Autom. Lett.*, vol. 3, no. 3, pp. 1426–1433, Jul. 2018.

[8] M. E. Nisser, S. M. Felton, M. T. Tolley, M. Rubenstein, and R. J. Wood, "Feedback-controlled self-folding of autonomous robot collectives," in *Proc. IEEE/RSJ Int. Conf. Intell. Robots Syst.*, 2016, pp. 1254–1261.

[9] W. P. Weston-Dawkes, A. C. Ong, M. R. A. Majit, F. Joseph, and M. T. Tolley, "Towards rapid mechanical customization of cm-scale self-folding agents," in *Proc. IEEE/RSJ Int. Conf. Intell. Robots Syst.*, 2017, pp. 4312–4318.

[10] S. A. Zirbel *et al.*, "Accommodating thickness in origami-based deployable arrays," *J. Mech. Des.*, vol. 135, no. 11, 2013, Art. no. 111005.

[11] S. Miyashita, S. Guitron, M. Ludersdorfer, C. R. Sung, and D. Rus, "An untethered miniature origami robot that self-folds, walks, swims, and degrades," in *Proc. IEEE Int. Conf. Robot. Autom.*, 2015, pp. 1490–1496.

[12] Q. Shi, X. Shi, J. M. Gattas, and S. Kitipornchai, "Folded assembly methods for thin-walled steel structures," *J. Constructional Steel Res.*, vol. 138, pp. 235–245, 2017.

[13] C. Quaglia, A. Dascanio, and A. Thrall, "Bascule shelters: A novel erection strategy for origami-inspired deployable structures," *Eng. Struct.*, vol. 75, pp. 276–287, 2014.

[14] S. Felton, M. Tolley, E. Demaine, D. Rus, and R. Wood, "A method for building self-folding machines," *Science*, vol. 345, no. 6197, pp. 644–646, 2014.

[15] C. Liu and S. M. Felton, "A self-folding robot arm for load-bearing operations," in *Proc. IEEE/RSJ Int. Conf. Intell. Robots Syst.*, 2017, pp. 1979–1986.

[16] W. Wang, J.-Y. Lee, H. Rodrigue, S.-H. Song, W.-S. Chu, and S.-H. Ahn, "Locomotion of inchworm-inspired robot made of smart soft composite (SSC)," *Bioinspiration Biomimetics*, vol. 9, no. 4, 2014, Art. no. 046006.

[17] K. Zhang, C. Qiu, and J. S. Dai, "Helical kirigami-enabled centimeter-scale worm robot with shape-memory-alloy linear actuators," *J. Mechanisms Robot.*, vol. 7, no. 2, 2015, Art. no. 021014.

[18] G. K. Klute, J. M. Czerniecki, and B. Hannaford, "Mckibben artificial muscles: Pneumatic actuators with biomechanical intelligence," in *Proc. IEEE/ASME Int. Conf. Adv. Intell. Mechatronics*, 1999, pp. 221–226.

[19] R. Niiyama, X. Sun, C. Sung, B. An, D. Rus, and S. Kim, "Pouch motors: Printable soft actuators integrated with computational design," *Soft Robot.*, vol. 2, no. 2, pp. 59–70, 2015.

[20] J. Yi, X. Chen, C. Song, and Z. Wang, "Fiber-reinforced origamic robotic actuator," *Soft Robot.*, vol. 5, no. 1, pp. 81–92, 2018.

[21] F. Renda, M. Giorelli, M. Calisti, M. Cianchetti, and C. Laschi, "Dynamic model of a multibending soft robot arm driven by cables," *IEEE Trans. Robot.*, vol. 30, no. 5, pp. 1109–1122, Oct. 2014.

[22] S.-J. Kim, D.-Y. Lee, G.-P. Jung, and K.-J. Cho, "An origami-inspired, self-locking robotic arm that can be folded flat," *Sci. Robot.*, vol. 3, no. 16, 2018, Art. no. eaar2915.

[23] S. Li, D. M. Vogt, D. Rus, and R. J. Wood, "Fluid-driven origami-inspired artificial muscles," *Proc. Nat. Acad. Sci.*, vol. 114, pp. 13132–13137, 2017.

[24] F. Connolly, P. Polygerinos, C. J. Walsh, and K. Bertoldi, "Mechanical programming of soft actuators by varying fiber angle," *Soft Robot.*, vol. 2, no. 1, pp. 26–32, 2015.

[25] L. Paez, G. Agarwal, and J. Paik, "Design and analysis of a soft pneumatic actuator with origami shell reinforcement," *Soft Robot.*, vol. 3, no. 3, pp. 109–119, 2016.

[26] R. Wood, E. Steltz, and R. Fearing, "Optimal energy density piezoelectric bending actuators," *Sensors Actuators A, Phys.*, vol. 119, no. 2, pp. 476–488, 2005.

[27] S. Russo, T. Ranzani, J. Gafford, C. J. Walsh, and R. J. Wood, "Soft pop-up mechanisms for micro surgical tools: Design and characterization of compliant millimeter-scale articulated structures," in *Proc. IEEE Int. Conf. Robot. Autom.*, 2016, pp. 750–757.

[28] J. Zhou, X. Chen, J. Li, Y. Tian, and Z. Wang, "A soft robotic approach to robust and dexterous grasping," in *Proc. IEEE Int. Conf. Soft Robot.*, 2018, pp. 412–417.

[29] X. Chen, J. Peng, J. Zhou, Y. Chen, M. Y. Wang, and Z. Wang, "A robotic manipulator design with novel soft actuators," in *Proc. IEEE Int. Conf. Robot. Autom.*, 2017, pp. 1878–1884.

[30] J. E. Shigley, *Shigley's Mechanical Engineering Design*. New York, NY, USA: McGraw-Hill, 2011.

[31] F. Collins and M. Yim, "Design of a spherical robot arm with the spiral zipper prismatic joint," in *Proc. IEEE Int. Conf. Robot. Autom.*, 2016, pp. 2137–2143.

[32] E. T. Filipov, T. Tachi, and G. H. Paulino, "Origami tubes assembled into stiff, yet reconfigurable structures and metamaterials," *Proc. Nat. Acad. Sci.*, vol. 112, no. 40, pp. 12321–12326, 2015.

[33] A. Yellowhorse, K. Tolman, and L. L. Howell, "Optimization of origami-based tubes for lightweight deployable structures," in *Proc. ASME Int. Des. Eng. Tech. Conf. Comput. Inf. Eng. Conf.*, 2017, Art. no. V05BT08A035.

[34] E. T. Filipov, G. H. Paulino, and T. Tachi, "Deployable sandwich surfaces with high out-of-plane stiffness," *J. Struct. Eng.*, vol. 145, no. 2, 2018, Art. no. 04018244.

[35] X. Sun, S. M. Felton, R. Niiyama, R. J. Wood, and S. Kim, "Self-folding and self-actuating robots: A pneumatic approach," in *Proc. IEEE Int. Conf. Robot. Autom.*, 2015, pp. 3160–3165.

[36] D. Kim and R. B. Gillespie, "Origami structured compliant actuator (OSCA)," in *Proc. IEEE Int. Conf. Rehabil. Robot.*, 2015, pp. 259–264.

[37] SPEEDAIRE, Speedaire—5PEH8. Dec. 04, 2018. [Online]. Available: https://www.grainger.com/product/SPEEDAIRE-3-4-Air-Cylinder-Bore-Dia-5PEH8

[38] H. McClintock, F. Z. Temel, N. Doshi, J.-S. Koh, and R. J. Wood, "The millidelta: A high-bandwidth, high-precision, millimeter-scale delta robot," *Sci. Robot.*, vol. 3, no. 14, 2018, Art. no. eaar3018.

[39] D. Morrison *et al.*,"Cartman: The low-cost cartesian manipulator that won the amazon robotics challenge," in *Proc. IEEE Int. Conf. Robot. Autom.*, 2018, pp. 7757–7764.

[40] K. Kim *et al.*, "Rapid prototyping design and control of tensegrity soft robot for locomotion," in *Proc. IEEE Int. Conf. Robot. Biomimetics*, 2014, pp. 7–14.